



Vertical distribution of wave shear stress in variable water depth: Theory and field observations

Qingping Zou,¹ Anthony J. Bowen,² and Alex E. Hay²

Received 17 September 2005; revised 18 May 2006; accepted 9 June 2006; published 26 September 2006.

[1] A generalized analytical model is developed to describe the vertical distribution of wave-induced shear stress in the presence of bottom slope, bottom friction and depth-induced wave breaking in the shoaling region and surf zone. The theory is compared to data obtained on an unbarred beach in 3.7-m mean water depth over a 2° bottom slope. Bottom slope and bottom friction are incorporated in the theory by including the wave energy dissipation by bottom friction in a potential wave theory for variable water depth, and coupling the wave theory with a wave bottom boundary layer (WBBL) theory over a sloping bottom. The effect of wave breaking is included through a periodic bore dissipation model. Previous studies have considered some, but not all, of these effects. Each of the three components, sloping bottom, bottom friction and wave breaking, exhibits a different vertical structure. The contributions due to bottom slope and bottom friction attain maximum strength in the WBBL, and decay with distance above the bed, approaching smaller but nonzero values at the surface. In contrast, the contribution from wave breaking is maximal at the surface, and decays linearly with depth, becoming zero at the bed. The vertical structure of the cross-shore (u) and vertical (w) components of wave orbital velocity was measured using a coherent Doppler acoustic profiler. The measured velocity fields were used to obtain the ensemble averaged wave shear stress profiles that extend across the WBBL to a height of 30 cm above the bed. Close to the seabed, the observed and predicted $\langle uw \rangle$ profiles are similar, confirming the sensitivity of wave stress to frictional and bottom slope effects within the WBBL. Farther from the bed, however, the observed profiles fall off more rapidly with height, as w approaches quadrature with u faster than predicted. Wave breaking induced shear stresses were not observed.

Citation: Zou, Q.-P., A. J. Bowen, and A. E. Hay (2006), Vertical distribution of wave shear stress in variable water depth: Theory and field observations, *J. Geophys. Res.*, *111*, C09032, doi:10.1029/2005JC003300.

1. Introduction

[2] Studies of wave-induced circulation have been motivated by its close coupling with sediment transport and subsequent morphological evolution through the shoaling region and surf zone. Along-shore and rip currents are the dominant feature of wave-induced circulation in the horizontal plane and have been investigated extensively by either 1-D or 2-D depth-averaged models [Bowen, 1969a, 1969b; Longuet-Higgins, 1970]. Wave-induced circulation in the cross-shore vertical plane is characterized by an offshore directed current, the undertow, which has been studied by 1-D or 2-D along-shore averaged models [Dyhr-Nielsen and Sorensen, 1970; Stive and Wind, 1986; Svendsen et al., 1987].

[3] However, recent studies suggest that along-shore and rip currents co-exist with cross-shore currents and that the vertical and horizontal variations of wave-induced circulation tend to intertwine on a natural beach [Svendsen and Lorenz, 1989; Svendsen and Putrevu, 1994]. It was also found that the vertical structure of nearshore circulation accounts for the order of magnitude enhancement of lateral mixing through nonlinear interactions of cross-shore and alongshore currents [Svendsen and Putrevu, 1994]. In addition, bottom currents that are directly related to sediment transport often deviate substantially from depth average currents in both direction and magnitude. Clearly, 3-D modeling is required to describe fully the dynamics of nearshore circulation and its contribution to sediment transport. Wave shear stress represents the vertical momentum flux within the circulation due to the presence of waves [Longuet-Higgins and Stewart, 1962]. It arises from the correlation between the horizontal and vertical wave velocities, which takes the form of $-\rho \langle uw \rangle$. Here $\langle \rangle$ signifies the time average and ρ is water density. It follows that the vertical distribution of wave shear stress is a central element

¹Centre for Coastal Dynamics and Engineering, School of Engineering, University of Plymouth, Plymouth, UK.

²Department of Oceanography, Dalhousie University, Halifax, Nova Scotia, Canada.

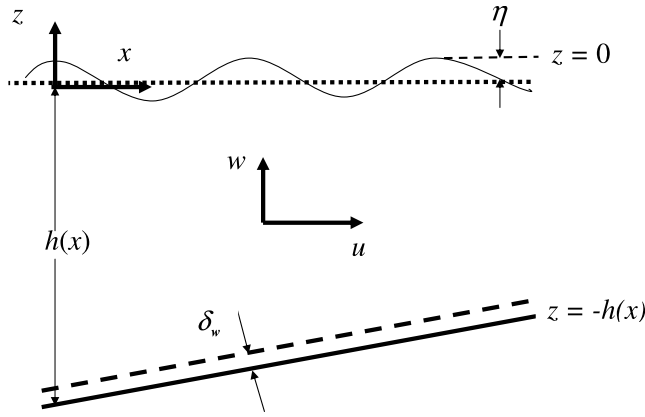


Figure 1. Definition sketch of variables and coordinate system for waves propagating over a planar, sloping seabed.

of 3-D modeling of wave-induced circulation, and this is the subject of this paper.

[4] Literature on the vertical distribution of wave shear stress is scarce, partly because the horizontal and vertical velocities given by the potential flow solution for waves propagating over a flat bed are in quadrature so that the wave shear stress is zero. In the presence of bottom slope, bottom friction and wave breaking, however, waves evolve as they propagate, therefore, the horizontal and vertical velocities are no longer in quadrature and a nonzero wave shear stress is induced.

[5] Previous studies of wave shear stress distribution have focused on the interior flow region and have not incorporated wave bottom boundary layers. Using a dynamic model of surface roller, *Deigaard and Fredsoe* [1989] constructed a theoretical solution for the shear stress of dissipative waves propagating over a horizontal bottom in shallow water. Through a sloping bottom perturbation of the linear wave solution for a horizontal bottom, *De Vriend and Kitou* [1990] obtained the wave shear stress solution for non-dissipative waves over a sloping bottom. Most recently, using the identity $\partial\langle uw \rangle / \partial z = \langle \zeta w \rangle - \partial[\langle u^2 \rangle - \langle w^2 \rangle] / \partial x / 2$, where $\langle uw \rangle$ is the wave shear stress, $\langle u^2 \rangle$ and $\langle w^2 \rangle$ are the wave normal stresses, $\zeta = u_z - w_x$ is the wave vorticity, subscripts “ x ” and “ z ” represent the derivative relative to x and z hereinafter, and invoking zero wave vorticity $\zeta = 0$ for the interior flow region, *Rivero and Arcilla* [1995] derived the shear stress solution for breaking or nondissipative waves over a sloping bed from the normal stress solutions for waves over a horizontal bottom. Their solution reduces to that of *Deigaard and Fredsoe* [1989] for breaking waves over a horizontal bottom in shallow water, and to that of *De Vriend and Kitou* [1990] for nondissipative waves over a sloping bottom in shallow water, but not in intermediate water depths.

[6] Here, we approach the theoretical problem differently: first, we extend *Chu and Mei*’s [1970] potential wave theory for a sloping bottom to incorporate wave bottom dissipation and wave breaking effects, match the velocity solutions with those of WBBL theory for a sloping bottom [*Zou and Hay*, 2003], and then obtain a matched wave shear stress solution for the full water column.

[7] Deviations of the phase between horizontal and vertical velocity components from 90° outside the WBBL have

been noticed in the field, from velocity measurements using current meters at different distances from the bed [*Herbers et al.*, 1992; *Elgar et al.*, 2001]. The viscous diffusion within boundary layers adjacent to solid and free surfaces also generates a nonzero wave shear stress which gives rise to a mean drift current [cf. *Longuet-Higgins*, 1960]. Despite that, field observations of shear stress profile have not been reported to our knowledge. This requires synoptic profile measurements of both velocity components, which has become available only recently using acoustic Doppler technique [*Zedel and Hay*, 1999]. In this study, the field observations over a 2° seabed slope at Queensland Beach, Nova Scotia, are compared with theoretical predictions of wave shear stress distribution to investigate the effects of bottom slope and WBBL.

[8] The objectives of this presentation are: (1) to develop a generalized solution of wave shear stress distribution incorporating the effects of bottom slope, bottom dissipation and wave breaking; (2) to examine in combination the effects of bottom slope, bottom dissipation and wave breaking, and (3) to compare the predicted wave shear stress profile with field measurements. Existing work considers some, but not all, of these effects. A secondary objective is to compare the present solution with previous results of *Deigaard and Fredsoe* [1989], *De Vriend and Kitou* [1990], and *Rivero and Arcilla* [1995].

2. Theory

[9] We consider here the vertical structure of shear stress beneath waves propagating over a sloping seabed, in finite depth of water, with a spatial scale of many wavelengths, i.e., $|\vec{\nabla}_H h| / kh = O(ka) \equiv O(\epsilon)$, where $\vec{\nabla}_H$ is the horizontal gradient operator, h is the water depth, k is the wave number, and a is the surface elevation amplitude.

[10] Following *Chu and Mei* [1970], we take x as the horizontal coordinate, positive shorewards, and z as the vertical coordinate, positive upward, with $z = 0$ at the mean free surface and $z = -h(x)$ at the bottom (see Figure 1). Through WKB expansions, the first harmonic solutions of a normally incident monochromatic wave over straight and parallel bottom contours are obtained as [cf. *Chu and Mei*, 1970; *Zou et al.*, 2003]

$$[U(x, z, t), W(x, z, t), \eta(x, t)] = \text{Re} \left\{ [U^{(1)}(X), W^{(1)}(X), \eta^{(1)}(X)] e^{i(kx - \omega t)} \right\}, \quad (1)$$

where $X = \epsilon x$ is the slowly varying horizontal coordinate, Re denotes the real part of the variable and superscript “(1)” denotes the complex amplitude of the primary wave hereinafter,

$$U^{(1)} = \frac{gak}{\omega \cosh q} [1 + i(\delta + \delta_u)] \cosh Q, \quad (2)$$

$$W^{(1)} = \frac{-igak}{\omega \cosh q} [(1 + i\delta) \sinh Q + i\delta_Q \cosh Q], \quad (3)$$

$$\eta^{(1)} = a, \quad (4)$$

where $Q = k(z + h)$, $q = kh$,

$$\delta = -[\alpha_1(Q - q) + \alpha_2(Q \tanh Q - q \tanh q) + \alpha_3(Q^2 - q^2)], \quad (5)$$

$$\delta_Q = -[\alpha_1 + \alpha_2(\tanh Q + Q \operatorname{sech}^2 Q) + 2\alpha_3 Q], \quad (6)$$

$$\delta_u = -[\alpha_2 + 2\alpha_3 Q \tanh Q + \alpha_1 \tanh Q], \quad (7)$$

where

$$\alpha_1 = h_x, \quad (8)$$

$$\alpha_2 = k^{-1} \left(\frac{a}{\cosh q} \right)^{-1} \left(\frac{a}{\cosh q} \right)_x, \quad (9)$$

$$\alpha_3 = \frac{k_x}{2k^2}, \quad (10)$$

α_1 , α_2 and α_3 are associated with the bottom topography, wave amplitude and wave number variations respectively and (9) and (10) may be rewritten as

$$\alpha_2 = \frac{1}{2kE} E_x - \frac{\tanh q}{1+G} h_x \quad (11)$$

and

$$\alpha_3 = \frac{-h_x}{2q} \frac{G}{1+G}, \quad (12)$$

where $G = 2q/\sinh(2q)$ and $E = \rho g a^2/2$ is the wave energy. According to (8) and (12), α_1 and α_3 are proportional to bottom slope h_x . As shown by equations (2) and (3), each velocity component is the corresponding horizontal bottom solution for nondissipative waves with added perturbation terms by bottom slope and wave energy gradient. Given by δ , δ_Q and δ_u , these perturbation terms are in quadrature with the horizontal bottom solutions for nondissipative wave, therefore, u and w are no longer in quadrature and a nonzero wave shear stress is induced.

[11] Assuming steady state, in the presence of bottom friction and wave breaking, wave transformation is governed by the wave energy flux balance equation

$$(C_g E)_x = -(D_f + D_b), \quad (13)$$

where D_f and D_b are the average rates of energy dissipation per unit area of seabed due to bottom friction and wave breaking, and $C_g = C(1 + G)/2$ and $C = \omega/k$ are the wave group and phase speeds respectively [Thornton and Guza, 1983].

[12] In addition to contributing to wave energy dissipation, bottom friction introduces a secondary vertical velocity

component, $-\tau_b/\rho C$, which arises from the velocity deficit within the wave bottom boundary layer (see Appendix B). The bed shear stress is given by

$$\tau_b = \frac{1}{2} \rho f_w |U_b^{(1)}| U_b, \quad (14)$$

where f_w is the friction factor, $U_b = U(z = -h)$ is the wave bottom velocity and $|U_b^{(1)}|$ is the wave bottom velocity amplitude. The secondary vertical velocity is 180° out of phase with the horizontal velocity, therefore, an additional wave shear stress is induced.

[13] Adding $-\tau_b^{(1)}/\rho C$ to the right hand side of (3) and combining it with (2), and invoking (5), (6) and (7), we obtain

$$\begin{aligned} \langle uw \rangle &= \operatorname{Re} \left(U^{(1)} W^{(1)*} \right) / 2 - \operatorname{Re} \left(U^{(1)} \tau_b^{(1)*} \right) / (2\rho C) \\ &= -G \frac{E}{\rho h} \left\{ [\alpha_1 + (\alpha_2 + 2\alpha_3) Q] + \frac{1}{2C} f_w |U_b^{(1)}| \cosh Q \right\} \end{aligned} \quad (15)$$

where superscript “*” denotes the complex conjugate hereinafter. Substituting (8), (11) and (12) into (15), we obtain

$$\begin{aligned} \langle uw \rangle &= -G \left(\frac{E}{\rho h} \right) \left[h_x - \frac{1}{1+G} \frac{q}{\tanh q} h_x \left(\frac{z+h}{h} \right) \right. \\ &\quad \left. + \frac{1}{2C} f_w |U_b^{(1)}| \cosh Q \right] - \frac{1}{2} G \frac{E_x}{\rho} \left(\frac{z+h}{h} \right) \end{aligned} \quad (16)$$

The above equation indicates that a positive/negative wave energy gradient E_x has a negative/positive contribution to $\langle uw \rangle$. As indicated in Figure 2, the shear stress solution (16) reduces to that of Rivero and Arcilla [1995] for breaking or nondissipative waves over a sloping bed, to that of De Vriend and Kitou [1990] for nondissipative waves over a sloping bottom and to that of Deigaard and Fredsoe [1989] for breaking waves over a horizontal bottom in shallow water.

[14] According to (14), the wave energy dissipation due to bottom friction is given by

$$D_f = \langle \tau_b U_b \rangle = \frac{1}{2} \rho f_w |U_b^{(1)}| \langle U_b^2 \rangle, \quad (17)$$

where $\langle U_b^2 \rangle = G \frac{E}{\rho h} + O(h_x)$ according to (2). Following Thornton and Guza [1983], we estimate the energy dissipation due to wave breaking by analogy with a traveling bore, that is

$$D_B = \frac{1}{4} \rho f g \frac{(BH)^3}{h}, \quad (18)$$

where f is the wave frequency, B is an empirical breaker coefficient of $O(1)$ and H is the wave height. Based on the assumption that the fluid velocity at the crest equals the phase speed for a Stokes wave, Miche (1954) proposed the breaker criterion

$$H_B = \frac{0.88}{k} \tanh \left(\frac{\gamma}{0.88} kh \right), \quad (19)$$

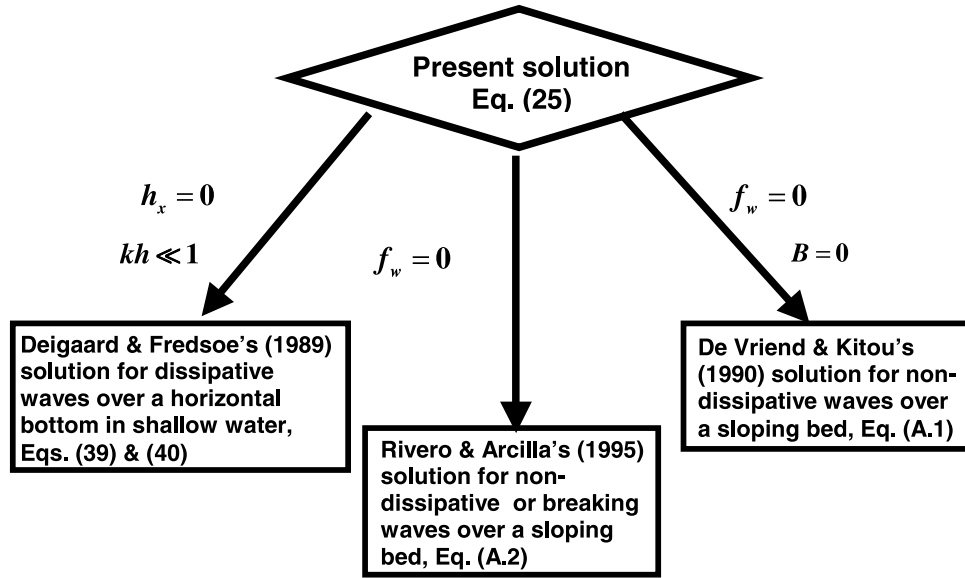


Figure 2. Comparisons of present solutions (25) and previous solutions by *Deigaard and Fredsoe* [1989], *Rivero and Arcilla* [1995], and *De Vriend and Kitou* [1990]. f_w is friction factor, B is the breaking coefficient, k is wave number, and $-h_x$ is the bottom slope.

where γ can vary from 0.4 to 1.2 depending on beach slope and breaker type. In shallow water where $kh \ll 1$, (19) becomes

$$H_B = \gamma h. \tag{20}$$

Invoking (13), (17) and (18), the coefficient α_2 defined by (11) may be decomposed into three components,

$$\alpha_2 = \alpha_{2s} + \alpha_{2f} + \alpha_{2B}, \tag{21}$$

where

$$\alpha_{2s} = -\frac{h_x}{(1+G)^2 \tanh q}, \tag{22}$$

$$\alpha_{2f} = \frac{-D_f}{2kC_g E} = -\frac{1}{2} \frac{f_w |U_b^{(1)}|}{C_g \sinh 2q}, \tag{23}$$

and

$$\alpha_{2B} = \frac{-D_B}{2kC_g E} = -(2\pi kh)^{-1} B^3 kH, \tag{24}$$

subscripts “s”, “f” and “B” represent the wave amplitude change due to shoaling, bottom friction and wave breaking. Substituting (21)–(24) into (15), we obtain

$$\begin{aligned} \langle uw \rangle &= -G \frac{E}{\rho h} \left\{ h_x \left[1 - \frac{1}{1+G} \frac{q}{\tanh q} \frac{z+h}{h} - \frac{G}{(1+G)^2} (1-q \tanh q) \frac{z+h}{h} \right] \right. \\ &\quad \left. + \frac{f_w |U_b^{(1)}|}{2C} \left[\cosh Q - \frac{CQ}{C_g \sinh 2q} \right] - (2\pi)^{-1} B^3 kH \frac{z+h}{h} \right\}. \end{aligned} \tag{25}$$

As indicated by (25), wave shear stress in the interior flow is the sum of three superimposed components due to bottom slope, bottom friction and wave breaking, represented as the first, second and third terms in the curly bracket of (25). According to (25), the bottom friction and wave breaking induced wave shear stresses are not sensitive to the bottom slope change. It is also evident from (15), (23) and (25), that bottom friction induced wave shear stress consists of two counteracting components with different vertical structure, while breaking induced wave shear stress comes solely from the negative wave energy gradient (24) due to breaking, therefore, is positive and has a linear vertical structure.

[15] The above solution is valid in the interior flow region ($z+h \geq z_b$), where z_b is a height several times greater than the boundary layer thickness. Within the WBBL ($z+h \leq z_b$), the solution takes the form of

$$\langle uw \rangle = \langle \hat{u} \hat{w} \rangle = \text{Re}(\hat{u}^{(1)} \hat{w}^{(1)*})/2, \tag{26}$$

where $\hat{u}^{(1)}$ and $\hat{w}^{(1)}$ are the complex amplitudes of the horizontal and vertical velocities for the WBBL over a sloping bottom, given by *Zou and Hay* [2003] (see Appendix B).

2.1. Bottom Slope Effects

[16] In the presence of a sloping bottom, the wave shear stress solution (25) reduces to

$$\begin{aligned} \langle uw \rangle &= -G \frac{E}{\rho h} h_x \left[1 - \frac{1}{1+G} \frac{q}{\tanh q} \frac{z+h}{h} \right. \\ &\quad \left. - \frac{G}{(1+G)^2} (1-q \tanh q) \frac{z+h}{h} \right] \end{aligned} \tag{27}$$

which displays a linear vertical distribution in the interior flow regardless of water depth relative to wavelength (see Figure 3). This is in contrast to the vertical distribution of

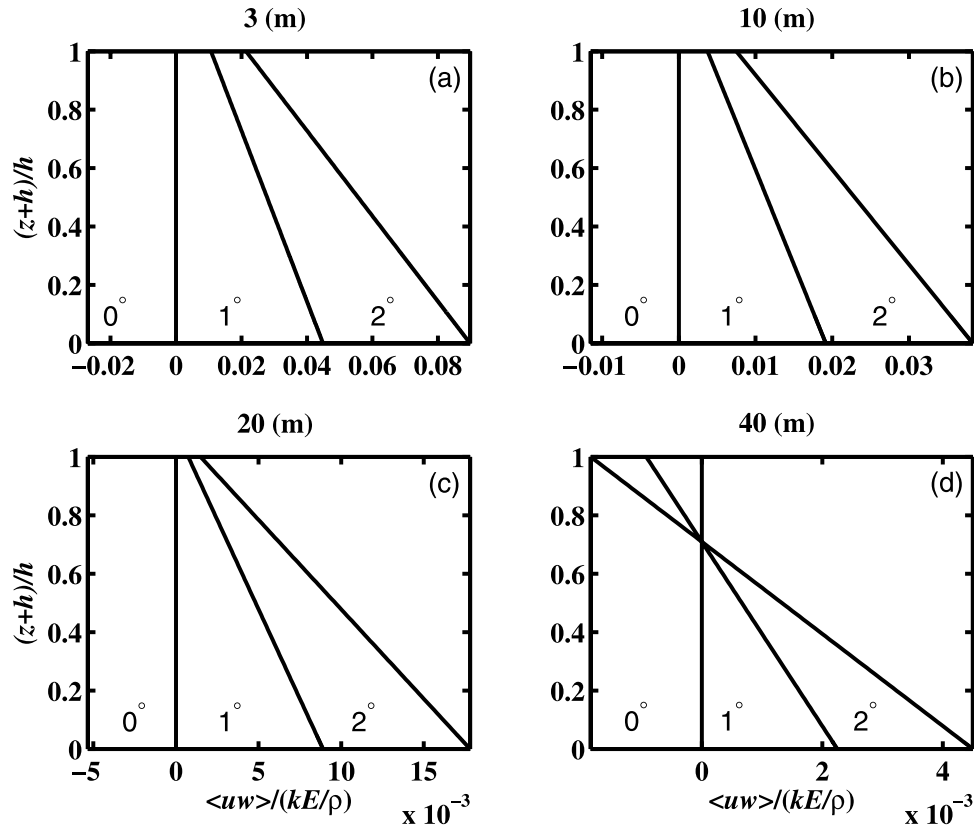


Figure 3. Predicted vertical profiles of normalized shear stress induced by a 10 s nonbreaking wave at a water depth of (a) 3 m, (b) 10 m, (c) 20 m and (d) 40 m using *Chu and Mei's* [1970] potential wave theory: predictions for a bed slope of 2° , 1° and 0° . The shear stress is normalized by kE where k and E are the wave number and wave energy.

wave normal stress, which is linear only if the water depth is much smaller than the wavelength [Zou *et al.*, 2003]. This result was explained by *Rivero and Arcilla* [1995] using a kinematic relationship

$$\langle uw \rangle_z = -\frac{1}{2} (\langle u^2 \rangle - \langle w^2 \rangle)_x. \quad (28)$$

Approximating the right hand side of the above relationship by the identity for irrotational flow over a horizontal bottom,

$$\langle u^2 \rangle - \langle w^2 \rangle = GE/\rho h \quad (29)$$

which is independent of the distance above the bed, so the vertical gradient of wave shear stress on the left hand side of (28) is independent of z .

[17] At the mean free surface, $z = 0$, the wave shear stress becomes

$$\langle uw \rangle = -\frac{GE}{\rho h(1+G)^2} (1-q \tanh q) h_x \quad (30)$$

and at the bottom, $z+h=0$, it becomes

$$\langle uw \rangle = -G \frac{E}{\rho h} h_x. \quad (31)$$

[18] As shown by Figure 3, the wave shear stress component due to bottom slope attains a maximum at the bed and decreases linearly with height toward a smaller, but nonzero value, at the surface. As discussed further in the following two paragraphs, the wave bottom shear stress is the product of bottom slope and wave bottom horizontal velocity variance, and the wave surface shear stress is one quarter of that value in shallow water and decreases with water depth toward zero in deep water (see Figure 4). As also indicated by Figure 3, at a given water depth and wave frequency, wave shear stress increases with bottom slope.

[19] For monochromatic waves, wave shear stress is related to wave velocities by

$$\langle uw \rangle = \langle u^2 \rangle^{1/2} \langle w^2 \rangle^{1/2} \cos \theta_{uw} \quad (32)$$

where θ_{uw} is the phase difference between u and w . Therefore, many of the features of the wave shear stress displayed in Figure 3 can be explained by the vertical variation of u and w , as demonstrated by *Zou et al.* [2003, Figure 2]: (1) the phase between u and w deviates from 90° throughout the water column and the deviation increases with bottom slope and toward the bed; (2) the sloping bottom effect on both the magnitude and phase of w decreases with height, increases with slope, and decreases with frequency for a given water depth; (3) bottom slope has little effects on the magnitude of u .

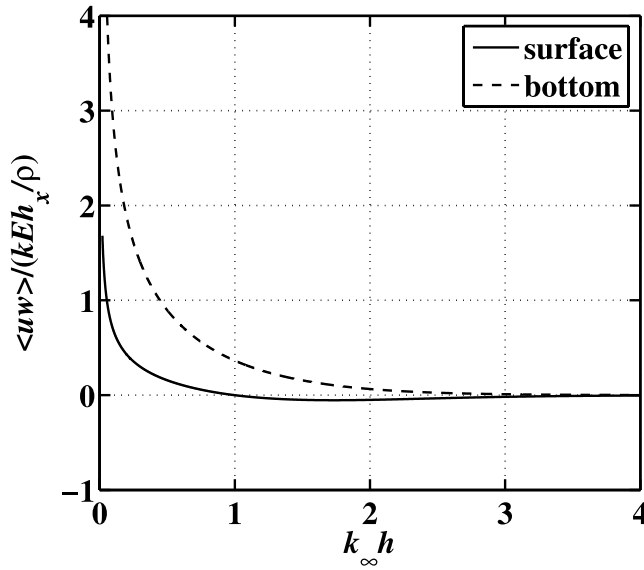


Figure 4. Normalized wave shear stress at the surface (solid line) and bottom (dashed line) for nonbreaking waves, as a function of the dimensionless water depth $k_\infty h$, where $k_\infty = \omega^2/g$ is deep water wave number. The shear stress is normalized by kEh_x where k , E and h_x are the wave number, wave energy and bottom slope.

[20] In order to satisfy the condition of no normal flow at the bed, $w = -h_x u$, the wave shear stress at the bottom becomes

$$\langle uw \rangle = -h_x \langle u^2 \rangle \equiv -GEh_x / \rho h \quad (33)$$

which is consistent with (31). The wave shear stress at the surface may be determined from the kinematic and dynamic conditions

$$w = \eta_t \quad (34)$$

and

$$\eta_x = -u_t / g \quad (35)$$

as

$$\begin{aligned} \langle uw \rangle &= \text{Re} \left(u^{(1)} w^{(1)*} \right) / 2 = g \eta^{(1)} \eta_x^{(1)*} / 2 = E_x / (2\rho) \\ &\equiv -GE(1 - q \tanh q) h_x / \left[\rho h (1 + G)^2 \right] \end{aligned} \quad (36)$$

which is consistent with (30). Thus the wave shear stress at the surface is half the wave energy gradient. This relationship indicates the presence of a nonzero surface shear stress in spatially nonuniform waves.

[21] For a given bottom slope, as the relative water depth, $k_\infty h$, increases, $\langle uw \rangle$ at the bottom (dashed line) decreases with the wave bottom velocity, whereas $\langle uw \rangle$ at the surface (solid lines) reduces to a negative value first and then slowly increases to zero in deep water (Figure 4). The latter effect, which looks peculiar, arises due to the theoretical decreases in wave height in intermediate depth during shoaling. It is also

evident from Figure 4 that $\langle uw \rangle$ at the surface is one quarter of its value at the bed in shallow water and that $\langle uw \rangle$ at the surface and at the bed decays toward zero at deeper water.

2.2. Bottom Friction Effects

[22] In the presence of bottom slope and bottom friction, the wave shear stress solution (25) reduces to

$$\begin{aligned} \langle uw \rangle &= -G \frac{E}{\rho h} \left\{ h_x \left[1 - \frac{1}{1 + G \tanh q} \frac{q}{h} \frac{z + h}{h} \right. \right. \\ &\quad \left. \left. - \frac{G}{(1 + G)^2} (1 - q \tanh q) \frac{z + h}{h} \right] \right. \\ &\quad \left. + \frac{f_w}{2C} \left| U_b^{(1)} \right| \left[\cosh Q - \frac{CQ}{C_g \sinh 2q} \right] \right\}. \end{aligned} \quad (37)$$

The second term in the curly bracket of (37) represents the bottom friction contribution to wave shear stress in the interior. The bottom friction induced $\langle uw \rangle$ is the sum of a negative component with a z -dependence of $\cosh Q$, given by the secondary vertical displacement $-\tau_b / \rho C$ due to the velocity deficit of WBBL and a positive component with a z -dependence of Q , contributed by the negative wave energy gradient due to bottom friction. The $\cosh Q$ term attains the same vertical structure as the horizontal velocity for a horizontal bottom while the Q term displays a linear vertical profile regardless of relative water depth. Throughout the interior region, the $\cosh Q$ term outweighs the Q term so that the net contribution to $\langle uw \rangle$ by bottom friction remains negative (see Figure 5). In addition, the bottom friction induced wave shear stress in the interior region is not sensitive to the bottom slope change.

[23] Within the WBBL, however, the wave shear stress distribution with bottom slope is distinct from that without slope (see Figure 5). More specifically, $\langle uw \rangle$ with bottom slope increases from zero at the bed to a local maximum and decreases slightly further upwards, whereas that without bottom slope decreases monotonically from zero at the bed to a negative value at the top of the layer (Figure 5). This is the result of a significant bottom slope effect on both the amplitude and phase of vertical velocity within the WBBL [cf. Zou and Hay, 2003, Figure 2].

2.3. Breaking Wave Effects

[24] In shallow water, the wave shear stress solution (25) reduces to

$$\begin{aligned} \langle uw \rangle &= -\frac{E}{\rho h} \left\{ h_x \left(1 - \frac{3z + h}{4h} \right) + (2C_g)^{-1} f_w \left| U_b^{(1)} \right| \left(1 - \frac{1z + h}{2h} \right) \right. \\ &\quad \left. - (2\pi)^{-1} B^3 kH \frac{z + h}{h} \right\} \end{aligned} \quad (38)$$

which is valid for shallow water waves subject to bottom slope, bottom friction as well as wave breaking effects.

[25] For a constant water depth and nonbreaking wave with bottom friction, (38) reduces to

$$\begin{aligned} \langle uw \rangle &= -f_w \left| U_b^{(1)} \right| \frac{E}{2\rho C_g h} \left(1 - \frac{1z + h}{2h} \right) \\ &= \frac{(E_x)_f}{\rho} \left(1 - \frac{1z + h}{2h} \right), \end{aligned} \quad (39)$$

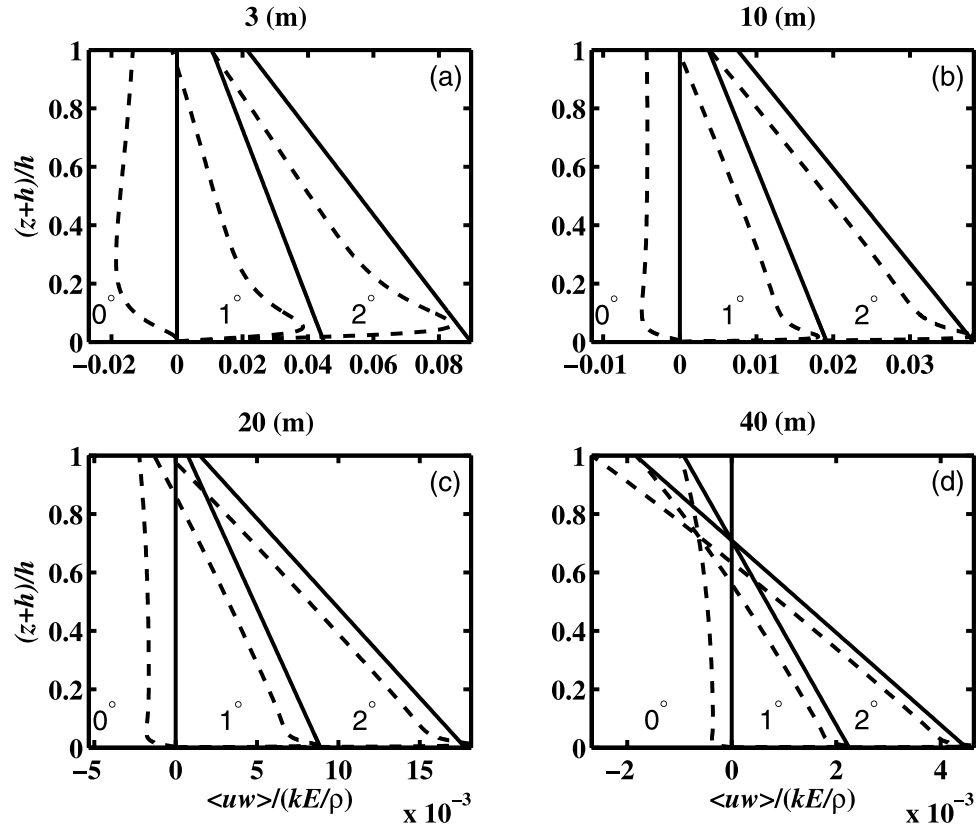


Figure 5. The predicted vertical profiles of the normalized shear stress induced by a 10 s nonbreaking wave at a water depth of (a) 3 m, (b) 10 m, (c) 20 m and (d) 40 m using the present theory with bottom friction (dashed line) and *Chu and Mei's* [1970] theory without bottom friction (solid line); predictions for a bed slope of 2° , 1° and 0° . The friction factor $f_w = 0.05$ and the wave bottom velocity amplitude $|U_b^{(1)}| = 1.17 \text{ ms}^{-1}$ are used in the predictions.

where $(E_x)_f = -D_f/C_g = -f_w|U_b^{(1)}|E/(2C_g h)$ is the wave energy gradient due to bottom friction, which is equivalent to equation (34) of *Deigaard and Fredsoe* [1989]. At the surface, the wave shear stress due to the secondary vertical displacement associated with the WBBL outweighs that due to wave bottom dissipation by a factor of two, so that (39) reduces to $\langle uw \rangle = \frac{1}{2\rho}(E_x)_f$. For a constant water depth and breaking waves without bottom friction, (38) reduces to

$$\begin{aligned} \langle uw \rangle &= (2\pi)^{-1} B^3 kH \frac{E z + h}{\rho h h} \\ &= -\frac{(E_x)_B z + h}{2\rho h}, \end{aligned} \quad (40)$$

where $(E_x)_B = -D_B/C_g = -\pi^{-1} B^3 kHE/h$ is the wave energy gradient due to wave breaking, which is equivalent to equation (52) of *Deigaard and Fredsoe* [1989]. At the surface, (40) reduces to $\langle uw \rangle = -\frac{1}{2}(E_x)_B/\rho$ which is consistent with (25).

[26] Wave breaking produces a negative wave energy gradient, which generates a positive $\langle uw \rangle$ (Figure 6). In contrast with the bottom slope induced wave stress, the wave breaking induced wave shear stress decreases with depth until it becomes zero at the bed (Figure 6). The opposing effects of wave breaking and bottom slope on the vertical gradient of wave shear stress introduce an additional

local minimum at the top of the WBBL. As also shown by Figure 6, wave breaking tends to enhance the local maximum of wave shear stress within the WBBL.

3. Field Measurements and Data Analysis

[27] The field measurements were carried out at Queensland Beach, Nova Scotia, an $O(100 \text{ m})$ -long, unbarred, pocket beach. The instrument deployment configuration is shown in Figure 7. An instrumented bottom pod was deployed approximately 60 m from the shoreline, in a mean water depth of 3.7 m. The local bed slope was about 2° with an accuracy of 0.5° according to rod and total station surveys and between 1.4° and 2.3° according to the rotary pencil beam sonar, during the storm. The seabed sediments were composed of fine sand with a median diameter of 0.17 mm. Vertical and horizontal velocity profiles with 0.7 cm vertical resolution were acquired at 15-minute intervals for about 8 minutes with a bistatic 1.7 MHz Coherent Doppler Profiler (CDP [*Zedel and Hay*, 1999]) at a profile acquisition rate of about 30 Hz, using 9 pulse-pair averaging. Surface elevation was measured at 30-minute intervals for about 8 min with an upward-looking, 2.25 MHz pencil beam acoustic sounder at a sampling rate of 8 Hz. Bedform geometry was detected at 30-minute intervals by cm-resolution 2.25 MHz rotary side scan and pencil beam sonars and continuously, except during daylight, with

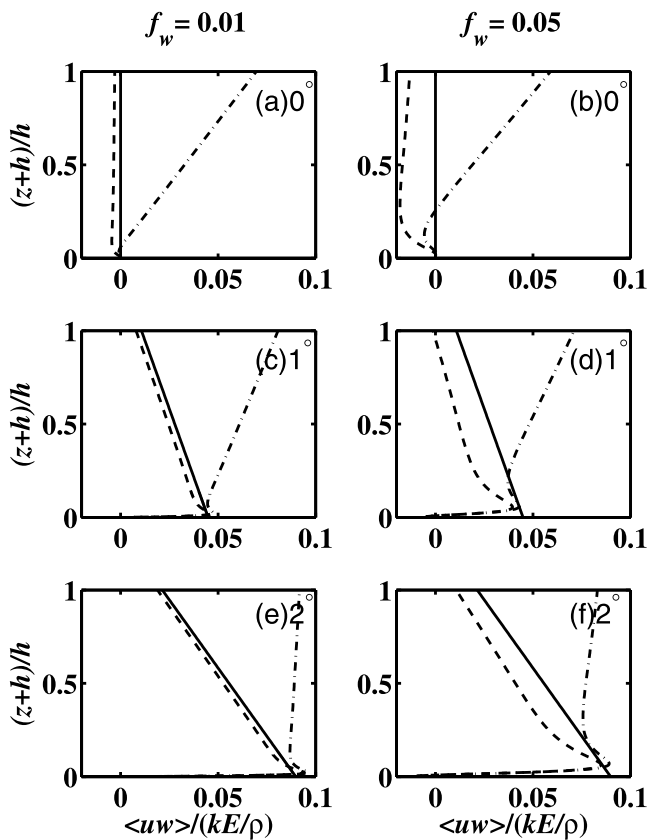


Figure 6. The predicted vertical profiles of the normalized shear stress induced by a 10 s breaking wave with a significant wave height of 1.5 m at a water depth of 3 m, over a bed slope of 0° (a and b), 1° (c and d), and 2° (e and f). The friction factor $f_w = 0.01$ (left panels), $f_w = 0.05$ (right panels) and wave breaking parameter $B = 1$ are used in the predictions. Prediction with wave breaking, bottom friction and bottom slope (dashed-dot line), bottom friction and bottom slope (dashed line), and only bottom slope (solid line).

a mm-resolution laser-video system. More detailed descriptions of the field site and instrumentation are given by Crawford and Hay [2001] and Smyth et al. [2002].

[28] Results are presented from three intervals during a storm event when the bed state changed from linear transition ripples to flat bed and then back to linear transition ripples before, during and after the peak of the storm [Crawford and Hay, 2001; Smyth et al., 2002]. Power spectra $S_{\eta\eta}$ of surface elevation η were estimated using Welch's averaged periodogram method and a Hanning window, dividing each 8-minute data run into demeaned and detrended 512-sample segments overlapped by 75%, which yields a degree of freedom of 28. As shown in Figure 8, the wave surface elevation spectrum, $S_{\eta\eta}$, was bimodal during storm growth and unimodal during storm decay. The evolution of wave spectra in Figure 8 reflects the transition of the wavefield from a mix of sea and swell immediately preceding and during storm peak to residual swell during storm decay.

[29] CDP measurements of horizontal and vertical velocity profiles extend to a height of about 30 and 50 cm above

the bed respectively. The measured u and w are bandpass filtered between 0.08 and 0.3 Hz using a 5th order Butterworth filter. The time averaged correlation between the filtered u and w is taken as the wave shear stress. Vertical profiles of wave shear stress and root-mean square vertical and horizontal wave orbital velocity are presented in Figures 9–11, for the three time intervals. Note that the horizontal velocity measurements close to the bed may be contaminated by the high-amplitude bottom reflection leaking into the received signal through the sidelobes of the transducer beam pattern. Thus, the lowest 3 points of $\langle uw \rangle$ and u_{rms} should be viewed with caution [see also Zou and Hay, 2003], a point to which we return in section 5.2.

[30] The $\langle uw \rangle$ profiles in these figures indicate an increase in the magnitude of wave stress with time as the storm builds, and then a gradual reduction as the storm decays. According to (33), the magnitude of $\langle uw \rangle$ near the bed would be expected to be $\sim u_{rms}^2 h_x$ in the absence of bottom friction. Thus, using the u_{rms} profile at 7:45 GMT in Figure 10c and a 2° bottom slope for example, the expected value of $\langle uw \rangle$ immediately above the WBBL would be $\sim 5 \times 10^{-3}$, which is comparable to the magnitude of the near-bottom peak for the corresponding $\langle uw \rangle$ profile in Figure 10a. Also evident in these figures is the steeper $\langle uw \rangle$ gradients in the interior (i.e. above the WBBL) as wave energy increases.

4. Comparisons Between Theory and Measurements

[31] The predicted vertical profiles of wave shear stress $\langle uw \rangle$ with bottom slope (solid lines) compare well with observations within the WBBL (circles), but the discrepancy increases with distance above the bed outside the WBBL (Figure 12). The predictions without bottom slope (dash-dotted lines), however, severely underestimate the observations in both these regions. Nobuoka and Mimura [2003] drew a similar conclusion from their comparisons of wave shear stress measured in a laboratory wave tank to Biesel and Airy wave theory. They also noticed that the observations of wave shear stress near wave breaking points are over estimated by theory and suggested that wave nonlinearity might contribute to the error. As shown by Figure 12, the observed wave shear stress is less than 5% below its predicted value within WBBL, but is over-predicted by an

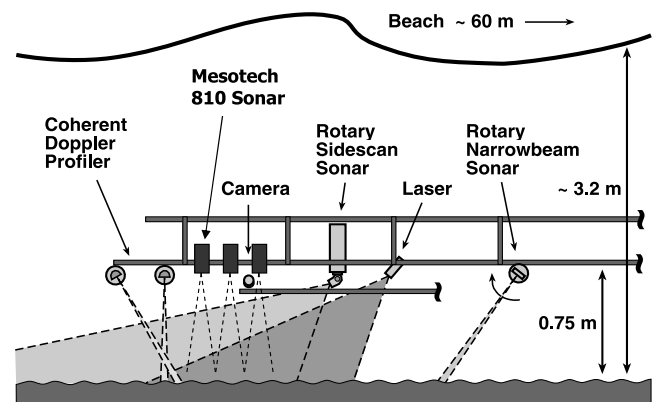


Figure 7. Side view of the instrument array configuration, adapted from Crawford and Hay [2001, Figure 4].

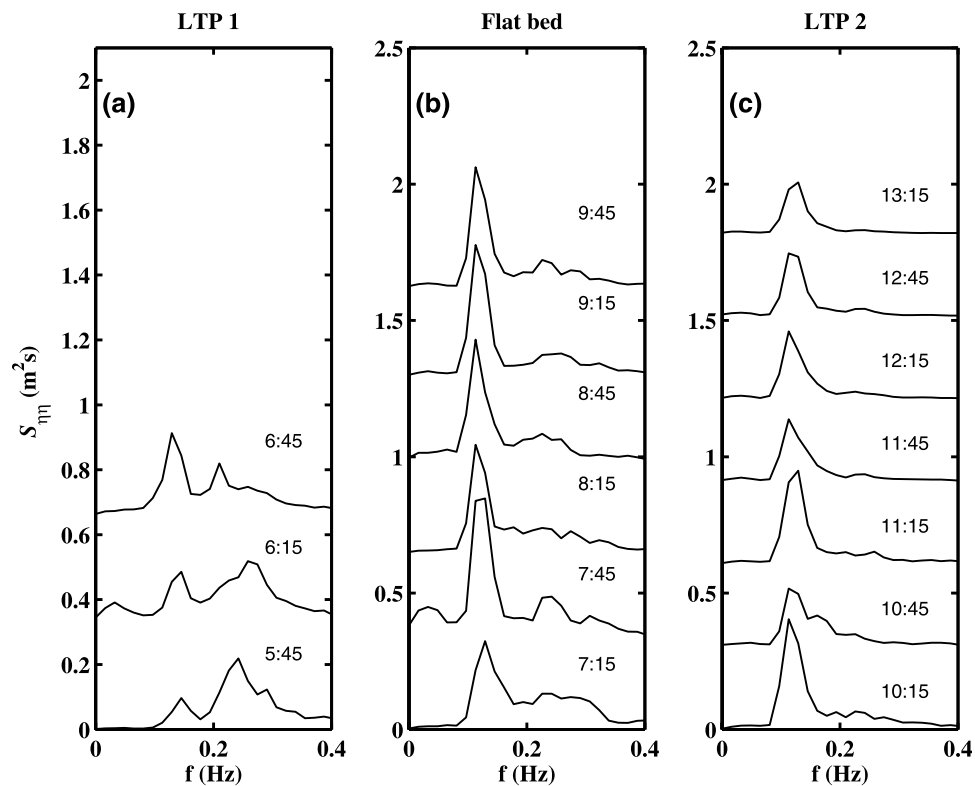


Figure 8. Surface elevation spectra, $S_{\eta\eta}$, with a degree of freedom of 28, during linear transition ripple I (left), flat bed (middle) and linear transition ripple II (right) intervals: spectra for each of the 8 minute data runs labeled with the starting time in GMT.

error that increases with height to about 50% at the uppermost point. Different from *Nobuoka and Mimura* [2003], the disparity remains the same for three intervals of different sea state. Thus, these data do not indicate that the discrepancy is due to wave nonlinearity.

[32] The observed local maximum of $\langle uw \rangle$ in the WBBL is accurately predicted by the sloping bottom theory with WBBL (solid line), but not by that without WBBL (dotted line), or that for a horizontal bottom (dash-dotted line). This result is consistent with that displayed by *Zou and Hay* [2003, Figure 9]; more specifically, same as vertical velocity, wave shear stress in the WBBL is subject to significant sloping bottom and turbulent friction effects.

[33] As shown by Figure 12, although the predicted wave shear stress is in good agreement with observations within the WBBL, the observed wave shear stress fall off more rapidly with height than predicted outside the WBBL. This result is consistent with that displayed by Figures 13c and 13d (same as Figure 5 of *Zou et al.* [2003]) where the observed w approaches quadrature with u faster with height than predicted. As also shown in Figure 12, the upward increase of the error in prediction is more severe in the flat bed interval when wave bottom velocity reaches its maximum. The deviation between theory and observations will be discussed further in the next section.

5. Discussion

5.1. Theory

[34] The wave shear stress component due to the bottom slope attains its maximum at the bed and decreases linearly

with distance from the bed toward a smaller but nonzero value at the surface (Figure 3). The bottom slope induced wave shear stress at the bed is the product of the bed slope and the variance of the horizontal wave bottom velocity. At the surface, the wave stress is one quarter of the bottom value in shallow water, decreases with increasing relative water depth, reduces to a negative value first and then slowly increases to zero in deep water (Figure 4). The latter effect, which looks peculiar, arises due to the theoretical decreases in wave height in intermediate depth during shoaling.

[35] Outside the WBBL, bottom friction tends to decrease the wave shear stress by almost the same amount regardless of bottom slope. Within the WBBL, in the presence of bottom slope, bottom friction causes the wave shear stress to rise to a local maximum as the bed is approached, and then to decrease to zero at the bed. In the absence of bottom slope, bottom friction decreases the wave shear stress monotonically toward zero at the bed (Figure 5).

[36] The contribution to $\langle uw \rangle$ from depth-induced wave breaking increases linearly with height from zero at the bed to a positive, maximum value at the surface. At the top of the WBBL, the upward increasing trend of $\langle uw \rangle$ from wave breaking starts to outweigh the upward decreasing trend from bottom friction and, as a result, a minimum in $\langle uw \rangle$ occurs (Figure 6).

[37] *Rivero and Arcilla* [1995] pointed out the inconsistency between their results and those of *De Vriend and Kitou* [1990] for intermediate water depths despite both results being consistent for shallow water. In contrast, we

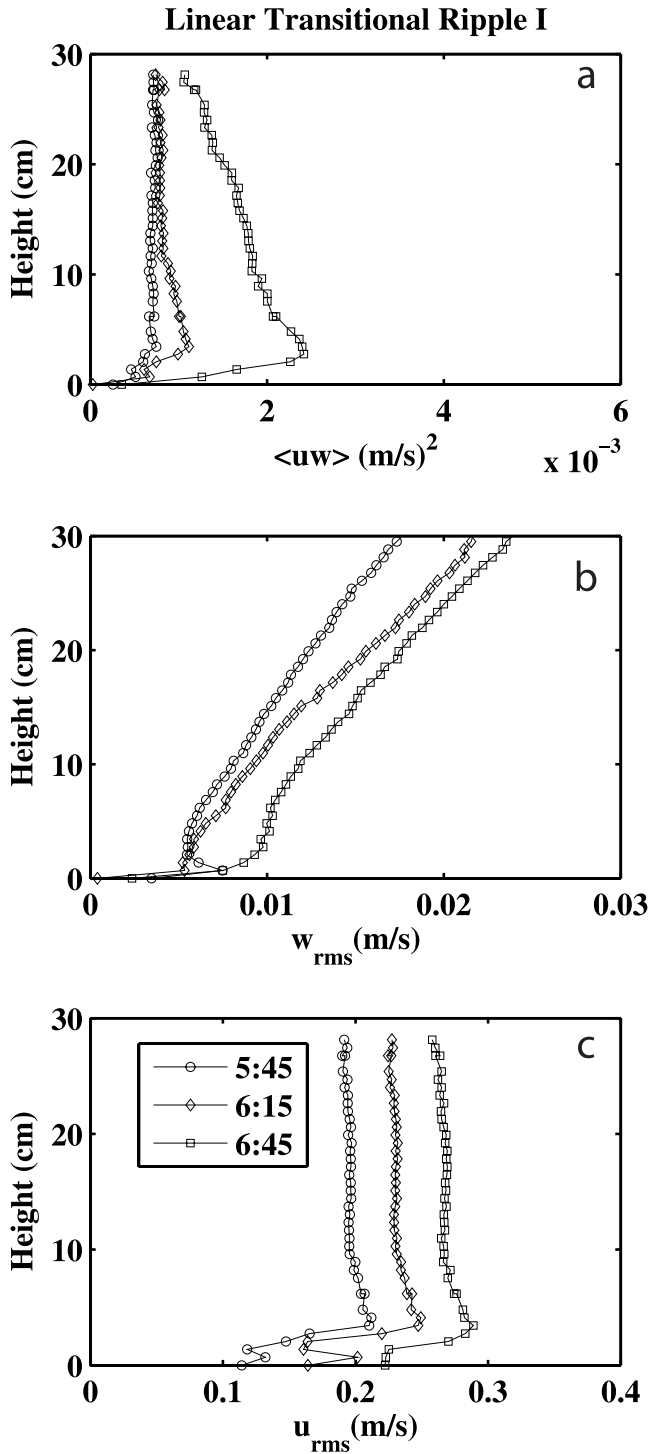


Figure 9. Time evolution of (a) wave shear stress $\langle uw \rangle$, root-mean square of (b) vertical and (c) horizontal velocity components during linear transition ripple I interval, where each of the 8 minute data runs are labeled with the starting time in GMT.

found that despite the difference in their approaches, these two sets of solutions are identical to each other (see Appendix A) and both are consistent with the present result.

[38] One may gain an insight into the role of wave shear stress in the momentum balance for nearshore circulation by combining the 1-D undertow equation by Svendsen [1984]

$$\frac{\langle \tau \rangle_z}{\rho} = g \langle \eta \rangle_x + (\langle u^2 \rangle - \langle w^2 \rangle)_x + \langle uw \rangle_z \quad (41)$$

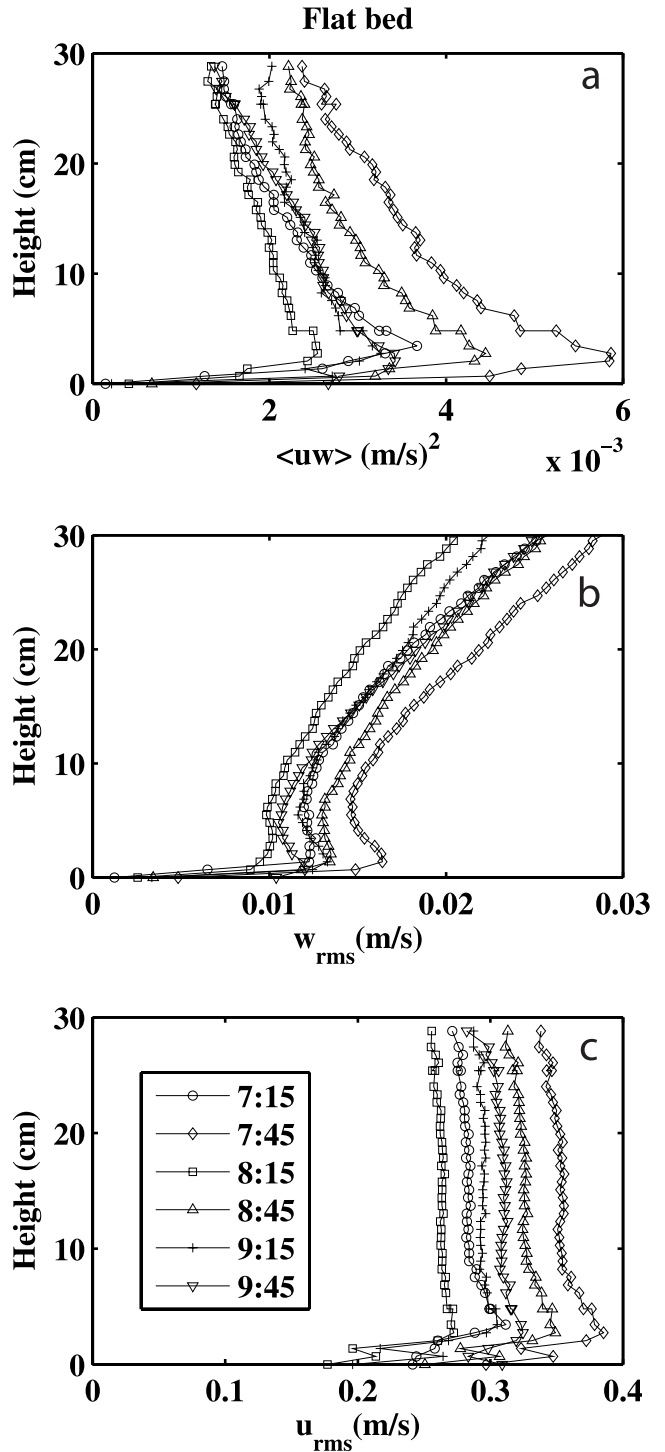


Figure 10. Same as Figure 9, except for the flat bed interval.

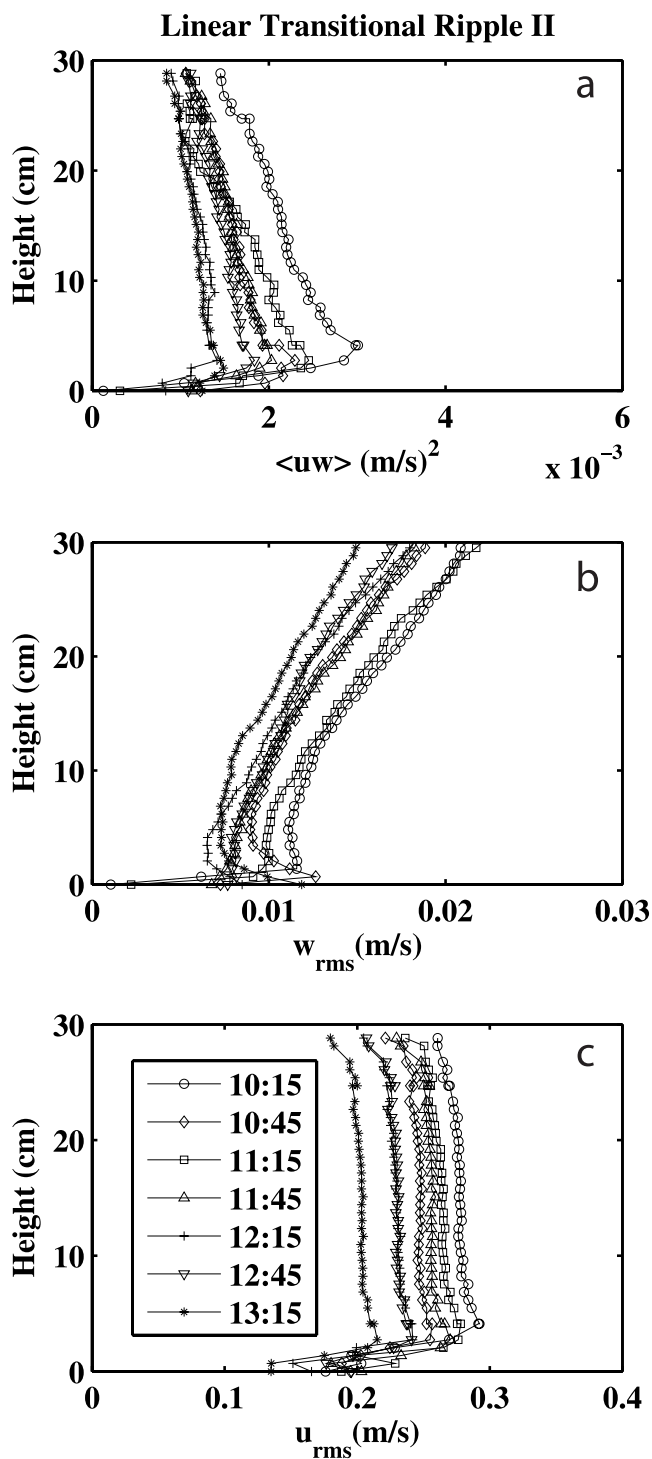


Figure 11. Same as Figure 9, except for the linear transition ripple II interval.

with the relationship (28), i.e., $\langle uw \rangle_z = -(\langle u^2 \rangle - \langle w^2 \rangle)_x / 2$ for the interior to obtain

$$\frac{\langle \tau \rangle_z}{\rho} = g \langle \eta \rangle_x + \frac{1}{2} (\langle u^2 \rangle - \langle w^2 \rangle)_x. \quad (42)$$

These equations indicate that the momentum flux generated by the wave shear stress is opposite in sign and half the

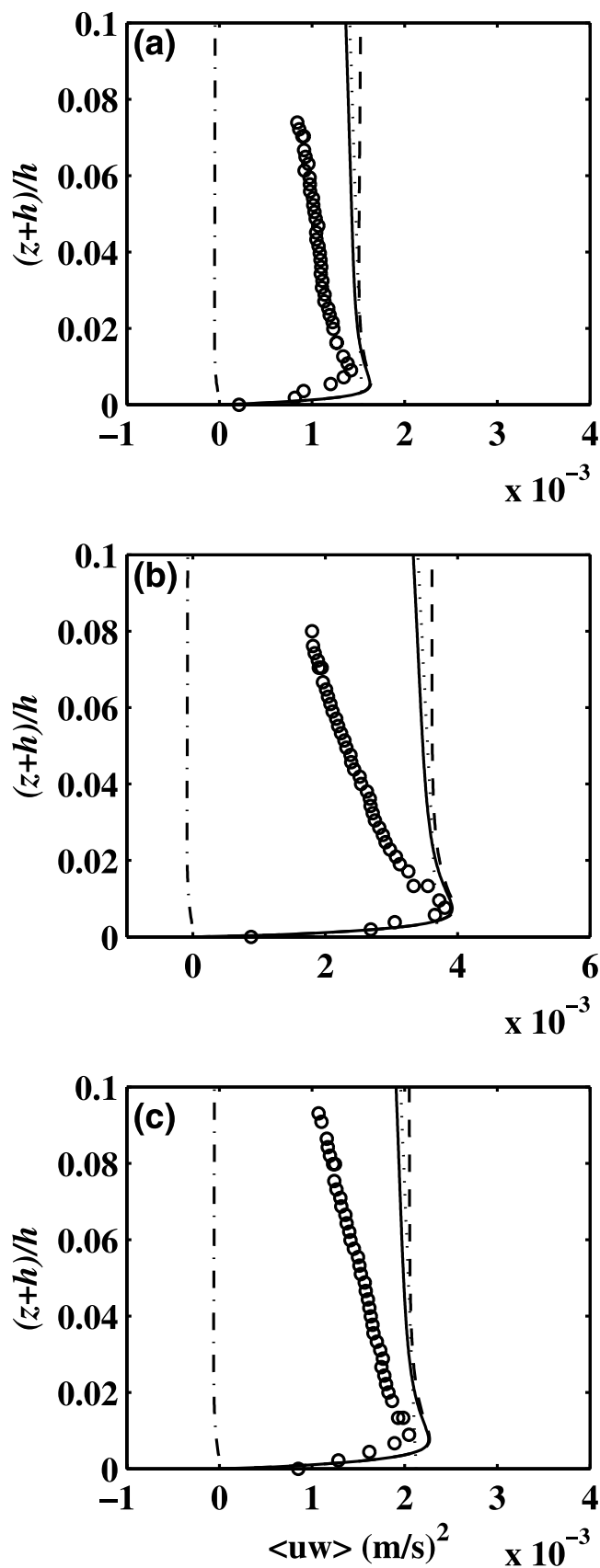
magnitude of that by wave normal stress. Since $(\langle u^2 \rangle - \langle w^2 \rangle)_x$ is normally smaller than $g \langle \eta \rangle_x$ within breaker region, the momentum flux induced by the wave shear stress has been neglected in previous studies of nearshore circulation until very recently. However, it is expected that wave shear stresses become significant in the mean flow momentum balance when $(\langle u^2 \rangle - \langle w^2 \rangle)_x$ attains a magnitude comparable to $g \langle \eta \rangle_x$, which often happens at the outer edge of the surf zone and in the shoaling region [Rivero and Arcilla, 1995].

5.2. Model-Data Comparisons

[39] Within the WBBL, the wave shear stress profiles are in good agreement with the predictions of the combined bottom slope/bed friction theory, notwithstanding the previously mentioned fact that the bottom-most 3 bins of the u -component profile are likely contaminated by the echo of the u_{rms} profiles, compared to w_{rms} , immediately above the bottom (Figures 10 and 11). The nearbed measurements of w are more reliable than u because of the CDP beam geometry. The w component is measured along a single, nearly vertical acoustic beam, whereas the u component is measured using the signal received by a transducer with its acoustic axis inclined away from vertical [Zedel and Hay, 1999; Smyth et al., 2002]. As a result of Fermat's principle of least time, and the sidelobes in the transducer beam patterns, a bottom echo can arrive at the inclined transducer before the relatively weaker signal scattered from particles in suspension within the range bins closest to the bed. In contrast, the earliest bottom echo in the vertical beam appears only in the bin defining the bed location. For the flat bed interval (Figure 10), the WBBL is about 5-cm thick, based on the w_{rms} profiles alone (also see Zou and Hay [2003] for WBBL thickness estimates). Thus, excluding the bottom-most 3 points from the $\langle uw \rangle$ profile, 5 or 6 measurement points are within the WBBL. Based on the comparisons of observations with theory in Figure 12b, these are just sufficient to resolve the nearbed peak in the wave shear stress.

[40] Despite the contamination of the bottom-most bins of the u -component profile by the bottom echo, there is still good agreement between the predicted and the ensemble-averaged $\langle uw \rangle$ profiles even very close to the bed (Figure 12). Thus, when averaged over a sufficient number of realizations, the ensemble-averaged $\langle uw \rangle$ exhibits the expected tendency toward zero at the bottom. Since $\langle uw \rangle$ relates to the variances of u and w by (32), it is likely that the near-bed $\langle uw \rangle$ gradient is mainly due to the rapid decay of $\langle w^2 \rangle^{1/2}$ toward zero at the bed, therefore, is not fully resolved by the 3 bottom-most data points.

[41] Outside the WBBL, none of the observed wave stress profiles exhibit any tendency toward higher stresses with increasing distance from the bottom, even during peak storm conditions. Neither do the predicted profiles indicate a tendency to increase away from the bed for the range of wave height spanned by the observations, using a wave breaking parameter $B = 1$. Thus, for the mean water depth of 3.67 m and significant wave heights up to 1.2-m observed by the experiment, the wave-breaking effects on $\langle uw \rangle$ did not penetrate to within 30 cm of the bed.



[42] Also outside the WBBL, the observed $\langle uw \rangle$ profiles decay with height much more rapidly than the predictions (Figure 12). $\langle uw \rangle$ is dependent on the phase between u and w (see (32)). Thus, this rapid decay is caused by the observed w approaching quadrature with the observed u much more rapidly than the predictions (Figure 13c). This might be generated by the flow blocking which tends to introduce a w perturbation that is phase-locked to u and increases toward the source of disturbance (Using results from tow-tank experiments with a similar CDP system, *Zedel and Hay* [2002] found that departures in the measured profiles from the uniform vertical structure expected in the tow tank could be explained by the blocking effect.). For the present experiment, the instruments were deployed on a cantilevered mast to avoid potential contamination of the nearby measurements by wakes from the frame legs. The CDP transceiver housings are cylindrical, ~ 10 cm in diameter and ~ 30 cm in length. Other sensor housings of comparable size were mounted shoreward of the CDP transceivers (Figure 7). Together, these instrument packages present a nonnegligible local obstruction to the flow.

[43] To estimate the effects of flow blocking, we combine potential flow around a sphere [*Kundu and Cohen*, 2004, section 5.19] with *Chu and Mei's* [1970] potential wave theory for a sloping bottom [*Zou et al.*, 2003]. Similar to *Zedel and Hay* [2002], the method of images is used to satisfy the condition of no normal flow at the bed. The combined instrument assemblage is taken to be a 30-cm diameter sphere. The spherical shape is clearly a crude approximation (Figure 7). The choice of 30-cm diameter was based on the 30-cm length of the CDP housings. Figures 14 and 15 illustrate the effect of such a sphere at 0.85-m height on the profiles of transfer function, H_{wp} , and the wave stress, $\langle uw \rangle$, for a monochromatic wave with a frequency of 0.12 Hz in 3.67-m water depth. These figures represent the flow blocking effects averaged over a full wave cycle, driven by the u – component of the flow alone. In the presence of flow disturbance, on the onshore side of the sphere center, $x > 0$, w increases in magnitude more rapidly (Figure 14a) and approaches quadrature with u , less rapidly upwards (Figure 14c), leading to the increased values of $\langle uw \rangle$ with height in Figure 15a. On the offshore side of the sphere center, the opposite occurs: w increases in magnitude less rapidly (Figure 14b) and approaches quadrature with u more rapidly (Figure 14d), leading to a more rapid decay of $\langle uw \rangle$ with height (Figure 15b).

[44] The spatial distribution of instrument housings on the mast is displayed by Figure 7, which suggests that vertical-beam CDP unit locates on the offshore side of the effective centre of the blocking sphere. It is for this geometry that

Figure 12. Predicted and ensemble-averaged observed vertical profiles of shear stress for (a) linear transition ripple interval I (b) flat bed interval and (c) linear transition ripple interval II, for 3, 6 and 7 data runs respectively, and for a bed slope of 1.50° , 2° and 1.65° respectively: theory with bottom friction and horizontal bed (dashed-dot lines), sloping bed with/without breaking (dashed/solid lines), with breaking but without bottom friction (dotted line); the observations are denoted with circles; breaking parameter $B = 1$.

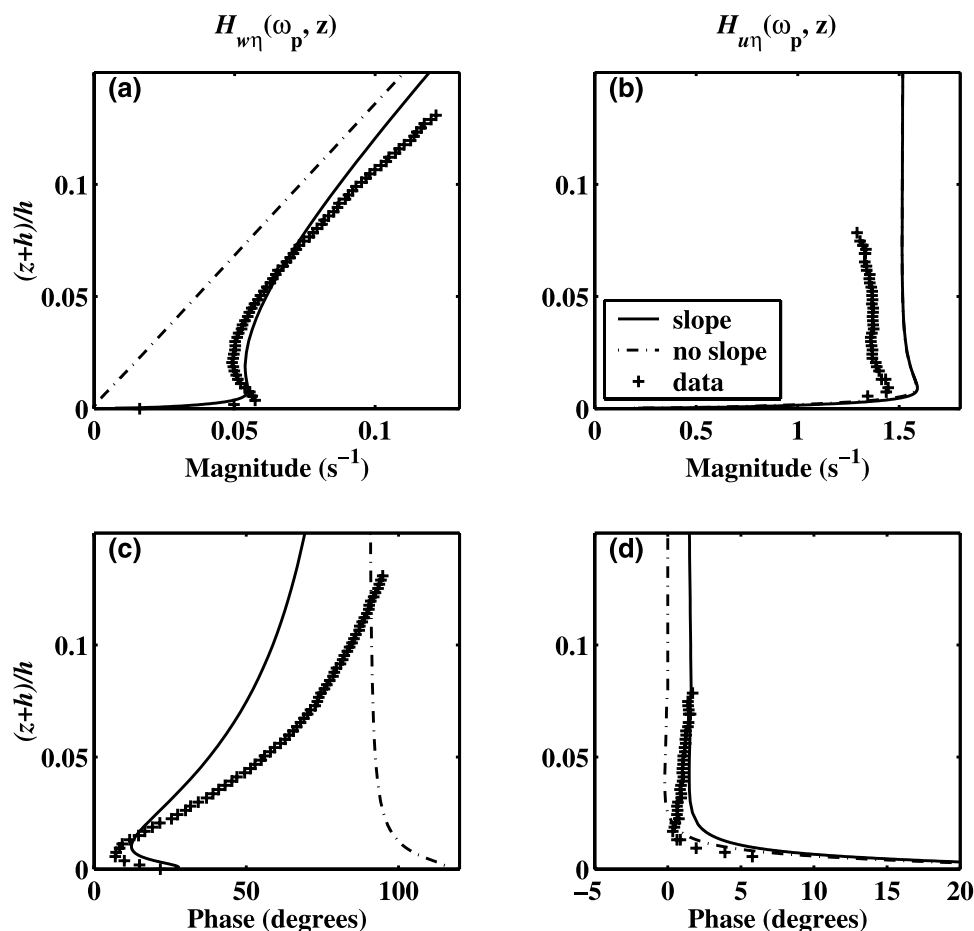


Figure 13. Vertical profiles of the magnitude and phase of the transfer functions $H_{w\eta}$ (a and c) and $H_{u\eta}$ (c and d) at the wave peak frequency for the flat bed interval: theory with bottom friction for a bed slope of 0° (dashed-dot lines) and 2° (solid lines); the observations are denoted with plus signs [after Zou *et al.*, 2003, Figure 5].

flow blocking is expected to cause $\langle uw \rangle$ to decrease more rapidly with height, which would explain the tendency of the observed $\langle uw \rangle$ to approach zero more rapidly with height than predicted (Figure 12). Similarly, the computed effect of flow blocking on $H_{w\eta}$ (Figure 14d) would explain the tendency for w to approach quadrature with u more rapidly in the observations than predicted (Figure 13c).

5.3. Wave Breaking Effects

[45] Measurements of the vertical profile of wave shear stress over a sloping bed have been made recently by De Serio and Mossa [2006] using Laser Doppler Velocimetry (LDV). Their experiments were carried out using regular waves, and their measured $\langle uw \rangle$ profiles extend from the outer shoaling region through the breaking region to the inner surf zone. Unlike the present study, these measurements did not resolve the WBBL. In the breaking region, De Serio and Mossa observed a linear increase of $\langle uw \rangle$ with height toward a maximum at the surface by wave breaking as predicted by the present theory.

[46] In the outer shoaling region, some of the De Serio and Mossa [2006] results (e.g. Test 1, Sect. 63) indicate a roughly linear decay of $\langle uw \rangle$ with height from a nearbed value of approximately $-h_x \langle U_b^2 \rangle$ to a near-zero value near

the surface, as predicted by the present sloping bed theory. While not all of the De Serio and Mossa $\langle uw \rangle$ profiles from the outer shoaling region exhibit this tendency consistently, none indicate the very rapid decay of $\langle uw \rangle$ with height seen in our data.

[47] Thus, the laboratory results of De Serio and Mossa [2006] support our conjecture that the rapid decay of $\langle uw \rangle$ with height in the field data might be an artifact of the measurement caused by the flow blocking of instrument packages. The computed blocking correction for the phase of w is similar to the departure of the observed phase from the sloping bed theory (Figures 13c and 14d), whereas the blocking correction for the magnitude of w is opposite to the departure of the observed magnitude from the prediction (Figures 13a and 14a). Despite that, the over-prediction of the observed $\langle uw \rangle$ in Figure 12 is mainly due to the error in the phase predictions of w that exclude the flow blocking effects.

6. Summary and Conclusions

[48] We have constructed a generalized solution for the wave shear stress distribution throughout the water column beneath dissipative and nondissipative waves in finite water

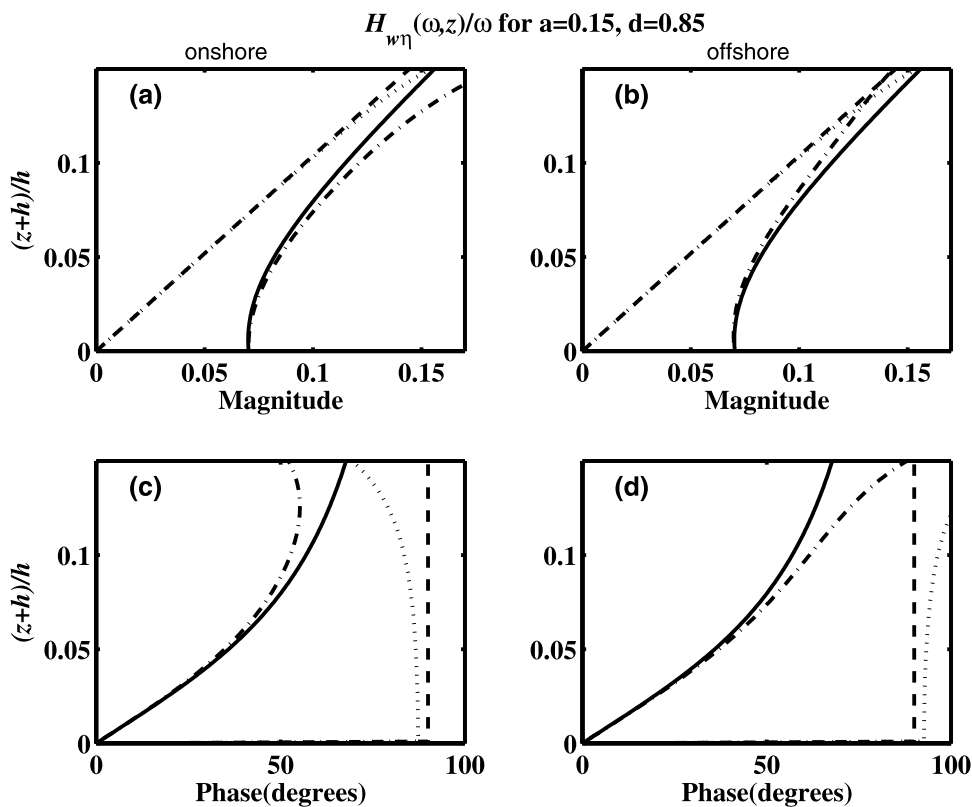


Figure 14. Vertical profiles of the magnitude and phase of the transfer functions between vertical velocity and surface elevation, $H_{w\eta}$, at 0.15 m onshore (a and c) and offshore (b and d) relative to the sphere center, at the wave peak frequency of 0.12 Hz. The results are shown for a sphere at 0.85 m above the bed, 0.15 m in radius. Theory with bottom friction for a bed slope of 0° with/without sphere (dotted/dashed lines) and 2° with/without sphere (dash-dotted/solid lines).

depth on a bottom slope, and have compared the theory to data from a field experiment on an unbarred beach. Bottom slope and bottom friction are incorporated in the theory using potential wave theory in combination with WBBL theory for a sloping bottom; wave breaking is included through a periodic bore dissipation model. In the interior flow region, the present solution reduces to that of *Deigaard*

and *Fredsoe* [1989] for the case of dissipative waves over a horizontal bottom in shallow water, to that of *Rivero and Arcilla* [1995] for the case of breaking waves or non-dissipative waves over a sloping bed, and to that of *De Vriend and Kitou* [1990] for the case of nondissipative waves over a sloping bed.

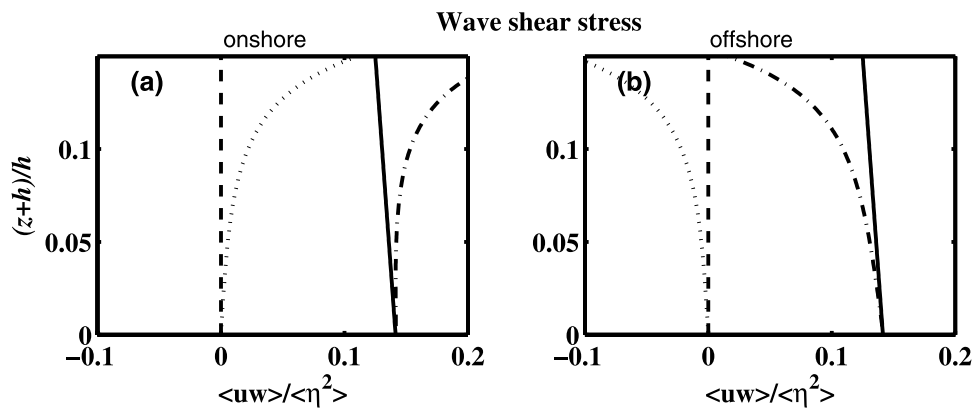


Figure 15. Same as Figure 14, except for the vertical profiles of wave shear stress. Theory with bottom friction for a bed slope of 0° with/without sphere (dotted/dashed lines) and 2° with/without sphere (dash-dotted/solid lines).

[49] The wave shear stress solution is the sum of three superimposed components due to the sloping bottom, bottom friction and wave breaking respectively. Bottom slope and wave breaking contribute a positive $\langle uw \rangle$, while bottom friction contributes a negative $\langle uw \rangle$. Each of these three components exhibits a different vertical structure. The bottom slope and bottom friction components are more pronounced near the bed, whereas the wave breaking contribution is enhanced near the surface. Outside the WBBL, the wave shear stress displays a linear vertical structure, whereas within the WBBL the wave shear stress increases from zero at the bed toward a local maximum and decreases farther away from the bed due to the combined effects of bottom friction and bottom slope.

[50] The present theory for a sloping bed gives reasonably good predictions of observed $\langle uw \rangle$ profile, while the theory for a horizontal bed severely underestimates the observations. More specifically, within the WBBL, the predicted $\langle uw \rangle$ profile is in good agreement with observations. Thus, both theory and observations illustrate the primary importance of WBBL and sloping bottom effects on the wave shear stresses close to the bed. In contrast, wave breaking effects on $\langle uw \rangle$ decrease toward zero at the bed. Consistent with the theory, the effects of breaking on the wave stress were not detectable in the observations for the range of conditions encountered in the experiment (i.e. $H_s/h \leq 0.32$) and the heights spanned by the $\langle uw \rangle$ profiles ($[z + h]/h < 0.1$).

[51] Outside the WBBL, the observed $\langle uw \rangle$ profiles decay more rapidly with height than the predictions. Potential flow analysis indicates that this discrepancy might be a consequence of flow blocking by the sensor housings. This conjecture is supported by recently published laboratory measurements, which do not exhibit such a rapid decay of $\langle uw \rangle$ with height.

Appendix A: *De Vriend and Kitou's* [1990] and *Rivero and Arcilla's* [1995] Results

[52] *Rivero and Arcilla* [1995] cited the following wave shear stress solution by *De Vriend and Kitou* [1990] for shoaling waves over a sloping bed [cf. *Rivero and Arcilla*, 1995, equation (1)]

$$\langle uw \rangle = G \left(\frac{E}{\rho h} \right) \left[\frac{\partial z_h}{\partial x} + \frac{1}{1 + G} \frac{kh}{\tanh(kh)} \frac{\partial h}{\partial x} \left(\frac{z - z_h}{h} \right) \right] - \frac{1}{2} G \frac{E_x}{\rho} \left(\frac{z - z_h}{h} \right) \quad (\text{A1})$$

where z_h is the bottom vertical coordinate. Alternatively, *Rivero and Arcilla* [1995] obtained the shear stress solution through the relationship between wave induced shear stress $\langle uw \rangle$, normal stresses $\langle u^2 \rangle$ and $\langle w^2 \rangle$, and vorticity, that is [cf. *Rivero and Arcilla*, 1995, equation (24)]

$$\langle uw \rangle = -G \left(\frac{E}{\rho h} \right) \frac{\partial d}{\partial x} - \frac{1}{2} \frac{\partial}{\partial x} \left(G \frac{E}{\rho h} \right) \left(\frac{z - z_h}{h} \right) \quad (\text{A2})$$

where d is the still water depth and h is the mean water depth. The authors then commented "this equation is, though similar, essentially different from the one presented

in *De Vriend and Kitou* [1990], given by equation (1) in this paper". Replacing d in (A2) with $-z_h$, we reduce (A2) to

$$\langle uw \rangle = G \left(\frac{E}{\rho h} \right) \frac{\partial z_h}{\partial x} - \frac{1}{2} \frac{\partial}{\partial x} \left(G \frac{E}{\rho h} \right) (z - z_h) \quad (\text{A3})$$

which may be further rewritten as

$$\langle uw \rangle = G \left(\frac{E}{\rho h} \right) \frac{\partial z_h}{\partial x} + \frac{1}{2} G \frac{E}{\rho h} \left(\frac{1}{h} \frac{\partial h}{\partial x} - \frac{1}{G} \frac{\partial G}{\partial x} - \frac{E_x}{E} \right) (z - z_h). \quad (\text{A4})$$

Invoking the relationship

$$\frac{1}{G} \frac{\partial G}{\partial x} = \frac{1}{h} \frac{\partial h}{\partial x} \frac{1 - 2q \coth(2q)}{1 + G}, \quad (\text{A5})$$

reduces (A4) to

$$\langle uw \rangle = G \left(\frac{E}{\rho h} \right) \frac{\partial z_h}{\partial x} + \frac{\partial h}{\partial x} \frac{1}{1 + G \tanh q} \left(G \frac{E}{\rho h} \right) \left(\frac{z - z_h}{h} \right) - \frac{1}{2} G \frac{E_x}{\rho} \left(\frac{z - z_h}{h} \right) \quad (\text{A6})$$

which is equivalent to solution (A1) given by *De Vriend and Kitou* [1990]. It is then readily seen that in the absence of bottom friction, (16) is equivalent to the solution (A6) of *De Vriend and Kitou* [1990] and therefore equation (24) of *Rivero and Arcilla* [1995].

Appendix B: Bottom Friction Effects

[53] In addition to its contribution to wave energy dissipation (17), bottom friction introduces a perturbation to the vertical velocity in the interior flow, which arises from the velocity deficit of the wave bottom boundary layer [*Longuet-Higgins*, 1953]. The vertical velocity solution within a WBBL over a bottom slope of h_x was obtained by *Zou and Hay* [2003],

$$\hat{w}_h^{(1)} = \left(1 + i \frac{U_{bx}^{(1)}}{kU_b^{(1)}} \right) \hat{w}_h^{(1)} - h_x \hat{u}^{(1)}, \quad (\text{B1})$$

where

$$\hat{w}_h^{(1)} = ik \left[\int_{-h}^z U_b^{(1)} dz + \frac{1}{i\omega\rho} (\tau^{(1)} - \tau_b^{(1)}) \right] \quad (\text{B2})$$

is the corresponding WBBL vertical velocity for a horizontal bottom, $U_b^{(1)}$ is the amplitude of the wave bottom velocity, $U_{bx}^{(1)}$ is the horizontal gradient of $U_b^{(1)}$, $\tau^{(1)}$ is the turbulent shear stress, $\tau_b^{(1)}$ is the turbulent shear stress at the bed, $\hat{u}^{(1)}$ is the horizontal velocity solution within the WBBL and superscript "(1)" denotes the complex amplitude of the primary wave.

[54] The following velocity solutions are found to be valid for the whole water column [cf. *Zou et al.*, 2003],

$$u^{(1)} = U^{(1)} \frac{\hat{u}^{(1)}}{U_b^{(1)}}, \quad \text{for } -h \leq z \leq 0 \quad (\text{B3})$$

$$w^{(1)} = \begin{cases} \hat{w}^{(1)}, & \text{for } -h \leq z \leq -h + z_b \\ W^{(1)}(z) - W^{(1)}(z = -h + z_b) + \hat{w}^{(1)}(z = -h + z_b), & \text{for } -h + z_b \leq z \leq 0. \end{cases} \quad (\text{B4})$$

where z_b is a height corresponding to several boundary layer thickness, $\hat{u}^{(1)}$ and $\hat{w}^{(1)}$ are the WBBL velocity solutions for a sloping bottom given by *Zou and Hay* [2003]:

$$\hat{u}^{(1)} = U_b^{(1)} \left[1 - \frac{F_1(\alpha, \zeta)}{F_1(\alpha, \zeta_0)} \right], \quad (\text{B5})$$

and

$$\hat{w}^{(1)} = U_b^{(1)} \left\{ ik\omega^{-1} \left(1 + i \frac{U_{bx}^{(1)}}{kU_b^{(1)}} \right) \left[\kappa u_* \zeta - i \frac{\tau^{(1)} - \tau_b^{(1)}}{\rho U_b^{(1)}} \right] - h_x \left[1 - \frac{F_1(\alpha, \zeta)}{F_1(\alpha, \zeta_0)} \right] \right\}, \quad (\text{B6})$$

where

$$\tau^{(1)} = \rho \kappa u_* U_b^{(1)} (F_1(\alpha, \zeta_0))^{-1} (1 + i\alpha\zeta)^{-\frac{1}{2}} \cdot \sqrt{i\zeta} \frac{\ker_1 2\sqrt{\zeta} + i\text{kei}_1 2\sqrt{\zeta}}{\ker 2\sqrt{\zeta_0} + i\text{kei} 2\sqrt{\zeta_0}} \quad (\text{B7})$$

is the complex shear stress amplitude,

$$F_1(\alpha, \zeta) = (1 + i\alpha\zeta)^{-\frac{1}{2}} \left[\frac{\ker 2\sqrt{\zeta} + i\text{kei} 2\sqrt{\zeta}}{\ker 2\sqrt{\zeta_0} + i\text{kei} 2\sqrt{\zeta_0}} + \frac{\alpha}{2} \sqrt{i\zeta} \frac{\ker_1 2\sqrt{\zeta} + i\text{kei}_1 2\sqrt{\zeta}}{\ker 2\sqrt{\zeta_0} + i\text{kei} 2\sqrt{\zeta_0}} (1 + i\alpha\zeta)^{-1} \right], \quad (\text{B8})$$

(ker, kei) and (\ker_1 , kei_1) are the zeroth- and first-order Kelvin functions, $\zeta = (z + h)/\delta_w$ is the stretched vertical coordinate, $\zeta_0 = z_0/\delta_w$, z_0 is bottom roughness, $\delta_w \equiv \kappa u_* / \omega$, $\kappa \approx 0.4$ is von Karman's constant, $u_* = \sqrt{|\tau_b|/\rho}$ is the friction velocity, ω is the wave radian frequency and $\alpha = 2$ is the turbulent relaxation coefficient in the viscoelastic-diffusion model [*Zou*, 2002].

[55] Invoking the boundary condition for potential wave theory, $W_b^{(1)} = -h_x U_b^{(1)}$ ($z = -h$) and integrating the mass conservation equation, $U_x^{(1)} + W_z^{(1)} = 0$ over the interval $(-h, -h + z_b)$, we obtain

$$W^{(1)}(z = -h + z_b) = ik \left(1 + i \frac{U_{bx}^{(1)}}{kU_b^{(1)}} \right) \int_{-h}^{z_b} U_b^{(1)} dz - h_x U_b^{(1)}. \quad (\text{B9})$$

Combination of (B1) and (B2) at $z = -h + z_b$ leads to

$$\hat{w}^{(1)}(z = -h + z_b) = ik \left(1 + i \frac{U_{bx}^{(1)}}{kU_b^{(1)}} \right) \left[\int_{-h}^{z_b} U_b^{(1)} dz - \frac{1}{i\omega\rho} \tau_b^{(1)} \right] - h_x U_b^{(1)}. \quad (\text{B10})$$

Subtracting (B9) from (B10), we obtain the secondary vertical displacement just outside the WBBL,

$$\hat{w}^{(1)}(z = -h + z_b) - W^{(1)}(z = -h + z_b) = - \left(1 + i \frac{U_{bx}^{(1)}}{kU_b^{(1)}} \right) \frac{\tau_b^{(1)}}{\rho C}, \quad (\text{B11})$$

where $1 + i \frac{U_{bx}^{(1)}}{kU_b^{(1)}} = 1 + O(h_x)$ so that (B11) is approximately the same as that for a horizontal bottom at the leading order. [56] Substituting (B11) into (B4) gives

$$w^{(1)} = \begin{cases} \hat{w}^{(1)}, & \text{for } -h \leq z \leq -h + z_b \\ W^{(1)} - \frac{\tau_b^{(1)}}{\rho C} & \text{for } -h + z_b \leq z \leq 0 \end{cases}. \quad (\text{B12})$$

Notation

a	surface elevation amplitude.
B	empirical breaker coefficient.
C_g	$= C(1 + G)/2$, wave group speed.
\bar{C}	$= \omega/k$, wave phase speed.
D_f	wave energy dissipation due to bottom friction.
D_B	wave energy dissipation due to wave breaking.
E	$= \rho g a^2/2$, wave energy density.
f	wave frequency.
f_w	friction factor.
G	$= 2q/\sinh(2q)$.
g	acceleration of gravity.
H	wave height.
h	water depth.
k	wave number.
k_∞	deep water wave number.
Q	$= k(z + h)$
q	$= kh$.
U	wave horizontal velocity of potential flow.
U_b	wave bottom velocity.
u	wave horizontal velocity.
\hat{u}	WBBL horizontal velocity for a sloping bottom.
W	wave vertical velocity for potential flow.
w	wave vertical velocity.
\hat{w}	WBBL vertical velocity for a sloping bottom.
\hat{w}_h	WBBL vertical velocity for a horizontal bottom.
$U^{(1)}, \hat{u}^{(1)}, W^{(1)}, \hat{w}^{(1)}$	complex velocity amplitude.
x	horizontal coordinate, positive shoreward.
z	vertical coordinate, positive upward, with $z = 0$ at the mean water surface.
z_b	a height corresponding to several boundary layer thicknesses.
z_0	bottom roughness length.
η	surface elevation of primary wave.

$\eta^{(1)}$	complex surface elevation amplitude.
α	turbulent relaxation coefficient.
δ_w	thickness of WBBL.
κ	von Karman constant.
τ	turbulent shear stress.
τ_b	turbulent shear stress at the bed.
$\tau^{(1)}, \tau_b^{(1)}$	complex stress amplitude.
ω	wave radian frequency.
Operators	
$\langle \rangle$	time average.
$ $	magnitude.
Subscripts	
*	complex conjugate.
x	horizontal gradient.
z	vertical gradient.
t	time derivative.
rms	root mean square value.

[57] **Acknowledgments.** We thank Steve Elgar for drawing our attention to a key reference, Len Zedel and Carolyn Smyth for the initial processing of CDP data, and Anna Crawford for the instrumentation drawing. This research was funded by the Coastal Sciences Program of the U.S. Office of Naval Research and the Natural Science and Engineering Research Council of Canada. We also thank Will Perrie and the Petroleum Research Atlantic Canada (PRAC) for their support during the latter stage of this work.

References

- Bowen, A. J. (1969a), The generation of longshore currents on a plane beach, *J. Mar. Res.*, *27*, 206–214.
- Bowen, A. J. (1969b), Rip currents: 1. Theoretical investigations, *J. Geophys. Res.*, *74*, 5467–5478.
- Chu, V. H., and C. C. Mei (1970), On slowly varying Stokes waves, *J. Fluid. Mech.*, *41*, 873–887.
- Crawford, A. M., and A. E. Hay (2001), Linear transition ripple migration and wave orbital velocity skewness: Observations, *J. Geophys. Res.*, *106*(C7), 14,113–14,128.
- Deigaard, R., and J. Fredsoe (1989), Shear-stress distribution in dissipative water-waves, *Coastal Eng.*, *13*(4), 357–378.
- De Serio, F., and M. Mossa (2006), Experimental study on the hydrodynamics of regular breaking waves, *Coastal Eng.*, *53*(1), 99–113.
- De Vriend, H. J., and N. Kitou (1990), Incorporation of wave effects in a 3D hydrostatic mean current model, *Delft Hydraul. Rep.*, H-1295.
- Dyhr-Nielsen, M., and T. Sorensen (1970), Some sand transport phenomena on coasts with bars, in *Proceedings of 12th Coastal Engineering Conference*, pp. 855–866, Am. Soc. of Civ. Eng., Reston, Va.
- Elgar, S., B. Raubenheimer, and R. T. Guza (2001), Current meter performance in the surf zone, *J. Atmos. Oceanic Technol.*, *18*, 1735–1746.
- Herbers, T. H. C., R. L. Lowe, and R. T. Guza (1992), Field observations of orbital velocities and pressure in weakly nonlinear surface gravity waves, *J. Fluid Mech.*, *245*, 413–435.
- Kundu, P. K., and I. M. Cohen (2004), *Fluid Mechanics*, 3rd ed., 759 pp., Elsevier, New York.
- Longuet-Higgins, M. S. (1953), Mass transport in water waves, *Philos. Trans. R. Soc. London, Ser. A*, *245*, 535–581.
- Longuet-Higgins, M. S. (1960), Mass transport in the boundary layer at a free oscillating surface, *J. Fluid Mech.*, *8*, 293–305.
- Longuet-Higgins, M. S. (1970), Longshore currents generated by obliquely incident sea waves, *J. Geophys. Res.*, *75*, 6778–6789.
- Longuet-Higgins, M. S., and R. W. Stewart (1962), Radiation stress and mass transport in gravity waves with applications to surf-beats, *J. Fluid Mech.*, *13*, 481–504.
- Nobuoka, H., and N. Mimura (2003), 3-D nearshore current model focusing on the effect of sloping bottom on radiation stresses, paper presented at 28th Coastal Engineering Conference, Cardiff, UK.
- Rivero, F. J., and A. S. Arcilla (1995), On the vertical-distribution of $(\tilde{u} \tilde{w})$, *Coastal Eng.*, *25*(3–4), 137–152.
- Smyth, C., A. E. Hay, and L. Zedel (2002), Coherent Doppler Profiler measurements of near-bed suspended sediment fluxes and the influence of bed forms, *J. Geophys. Res.*, *107*(C8), 3105, doi:10.1029/2000JC000760.
- Stive, M. J. F., and H. G. Wind (1986), Cross-shore mean flow in the surf zone, *Coastal Eng.*, *10*, 325–340.
- Svendsen, I. A. (1984), Mass flux and undertow in the surf zone, *Coastal Eng.*, *8*, 347–365.
- Svendsen, I. A., and R. S. Lorenz (1989), Velocities in combined undertow and longshore currents, *Coastal Eng.*, *13*(1), 55–79.
- Svendsen, I. A., and U. Putrevu (1994), Nearshore mixing and dispersion, *Proc. R. Soc. London, Ser. A*, *445*, 561–576.
- Svendsen, I. A., H. A. Schaffer, and J. B. Hansen (1987), The interaction between the undertow and boundary layer flow on a beach, *J. Geophys. Res.*, *92*, 11,845–11,856.
- Thornton, E. B., and R. T. Guza (1983), Transformation of wave height distribution, *J. Geophys. Res.*, *88*, 5925–5938.
- Zedel, L., and A. E. Hay (1999), A coherent Doppler profiler for high resolution particle velocimetry in the ocean: Laboratory measurements of turbulence and particle flux, *J. Atmos. Oceanic Technol.*, *16*, 1102–1117.
- Zedel, L., and A. E. Hay (2002), A three component bistatic coherent Doppler velocity profiler: Error sensitivity and system accuracy, *IEEE J. Oceanic Eng.*, *27*, 717–725.
- Zou, Q.-P. (2002), An analytical model of wave bottom boundary layers incorporating turbulent relaxation and diffusion effects, *J. Phys. Oceanogr.*, *32*(9), 2441–2456.
- Zou, Q.-P., and A. E. Hay (2003), The vertical structure of the wave bottom boundary layer over a sloping bed: Theory and field measurements, *J. Phys. Oceanogr.*, *33*(7), 1380–1400.
- Zou, Q.-P., A. E. Hay, and A. J. Bowen (2003), The vertical structure of surface gravity waves propagating over a sloping seabed: Theory and field measurements, *J. Geophys. Res.*, *108*(C8), 3265, doi:10.1029/2002JC001432.

A. J. Bowen and A. E. Hay, Department of Oceanography, Dalhousie University, Halifax, NS, Canada B3H 4J1.

Q.-P. Zou, Centre for Coastal Dynamics and Engineering, School of Engineering, University of Plymouth, Plymouth PL4 8AA, UK. (qingping.zou@plymouth.ac.uk)